Received 20 November 2017
Revised 25 March 2018
26 May 2018
Accepted 31 May 2018

Permanent magnet shaping for cogging torque and torque ripple reduction of PMSM

Brahim Ladghem Chikouche
Département de Génié Electrique, Faculté de Technologie, Université de M'sila, M'sila, Algeria, and

Kamel Boughrara and Rachid Ibtiouen
Laboratoire de Recherche en Electrotechnique (LRE), Ecole Nationale Polytechnique, Algiers, Algeria

Abstract

Purpose – This paper aims to the improvement of permanent magnet shape in the popular permanent magnet synchronous machine (PMSM) is proposed in this paper in view to mitigate cogging torque magnitude and torque ripple.

Design/methodology/approach – A two-dimensional exact analytical approach of magnetic field distribution is established for the PMSM considering magnet shape and slot opening. The optimal magnet shape is constituted of small number of layers stacked radially. The thickness of each magnet layer is considered equal to about one mm or more; however, a parametric study was performed to determine pole pitch ratio value. The finite element method is used to validate the analytical results.

Findings – Cogging torque peaks and torque ripples can be mitigated significantly more than 90 per cent compared to results issued from machine having classical magnet shape. Raising the number of magnet layers can give better results. The results of this paper are compared also with those issued from the machine having sinusoidal magnet shape and give a good solution.

Originality/value – A new technique for cogging torque and torque ripple mitigation is proposed in this paper by changing permanent magnet shape. The proposed final magnet shape is constituted of a set of stacked and well-dimensioned layers relative to the opening angle.

Keywords Finite element analysis, Cogging torque, Analytical solution, Permanent magnet shaping, Torque ripples

Paper type Research paper

1. Introduction

The permanent magnet brushless machines are widely used in different fields of industry and domestic products as they offer outstanding performance advantages. The performances of these machines are influenced by different parameters such as cogging torque peak and torque ripple. The torque ripples are because of the interactions between the harmonics of the distorted sinusoidal back-electromotive force (EMF) and the harmonics of armature currents driven into the machine. However, the cogging torque exists even in open circuit which is because of the interaction between the permanent magnets of the rotor and the stator teeth. It is an additive factor which generates more noise and mechanical vibration in permanent magnet motor when it runs especially at lower speeds.

The previous studies on the mitigations or suppression of cogging torque or electromagnetic torque ripple for high performance applications are proposed by analytical

COMPEL - The international journal for computation and mathematics in electrical and electronic engineering
Vol. 37 No. 6, 2018
pp. 2232-2248

0332-1649
DOI 10.1108/COMPEL-11-2017-0482

approach or finite element method (FEM). The machine parameters affecting the cogging torque magnitude are numerous. These parameters depend on magnets shape and its magnetization direction (Fei and Luk, 2012; Jang *et al.*, 2011; Laskaris and Kladas, 2011; Wang *et al.*, 2014a), segmentation of permanent magnets (Ashabani *et al.*, 2011; Lateb *et al.*, 2006), stator teeth shape (Islam *et al.*, 2004; Sung *et al.*, 2011; Oner *et al.*, 2015), asymmetric distribution of magnets or slots (Wang *et al.*, 2013; Xintong *et al.*, 2009), fractional number of slots per pole (Wang *et al.*, 2014b; Zhu, 2015) and stator slots or the rotor magnets skewing (Xia *et al.*, 2015; Sadeghi and Parsa, 2012). Numerous researches using advanced control algorithms have been also introduced to mitigate vibrations due to electromagnetic torque ripple by improving back-EMF and current waveform; the objective of these research studies is to adapt both waveform (Gu *et al.*, 2018; Gong *et al.*, 2014; Houari *et al.*, 2018; Zhao and Yang, 2011).

In this paper, a comprehensive analytical approach incorporating Maxwell equations is used to analyze the air-gap field distribution in surface-mounted permanent magnet machine. A novel magnet shape having small number of layers staked radially is proposed in view to improve cogging torque and torque ripple. In addition, the influence of the number of poles and slots is also investigated with respect to stator and rotor topologies, electricals parameters and magnet remanence. The results of this paper are compared also with those issued from the machine having sinusoidal magnet shape. Finally, the results of analytical method are verified by linear FEM.

2. Optimal torque calculation

In this paper, the permanent magnet shape is configured to reduce cogging torque magnitude (Tc) and torque ripples (τ_{TT}). The magnet shape is divided into Nc layers stacked radially as shown in Figure 1. The magnet arc to pole pitch ratio of each magnet layer can be adjusted separately.

In the first step, we suppose that all machines are constrained by the same topologies of stator and rotor, where its dimensions are indicated in Table I, electrical parameters and magnet remanence. In the second step, the building of the magnet begins by assuming that all magnet layers have identical arc to pole pitch ratio value. The thickness of the magnet region is equal to Ea and the thickness of each magnet layer is equal to Eb

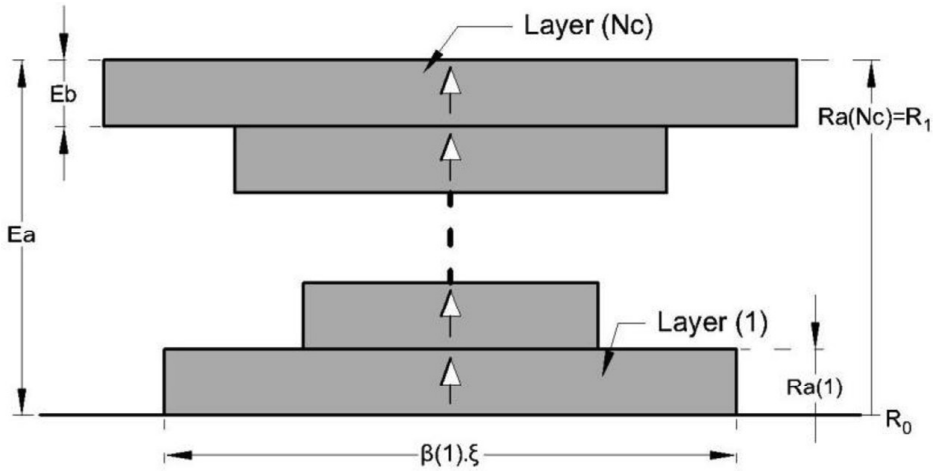

Figure 1.
Dividing the magnetic pole into Nc layers

Symbol	Parameter (unite)	Value
Brm	Max of magnet remanence (T)	1.28
–	Magnetization direction	Radial
p	Number of pole pairs	Variable
Qs	Number of stator slots	Variable
Nc	Number of layers of magnet	Variable
*R*0	Outer rotor radius (mm)	57.50
*R*1	Outer magnet radius (mm)	64.00
*R*2	Stator bore radius (mm)	64.65
*R*3	Inner stator slot radius (mm)	66.65
*R*4	Outer stator slot radius (mm)	92.65
Ea	Rotor magnet thickness (mm)	06.50
e	Air-gap length (mm)	00.65
*w*1	Slot opening (deg)	2
Ns	Number of turns per slot	10
Nh	Harmonics number	79

Table I.
Parameters of studied permanent-magnet motors

as indicated in Figure 1. For these conditions, we find the optimal opening of these magnet layers which gives an optimal cogging torque and thereafter an optimal torque ripple. The third step finds the optimal opening of other magnet layers simultaneously between 1 Nc − i where *i* represents the rank of magnet layer. This process is repeated until i = (Nc − 1). The number of layers should be also small, and the thickness of each magnet layer is equal to about 1 mm or more. Figure 2 shows the algorithm where we can follow it to give final shape of magnet.

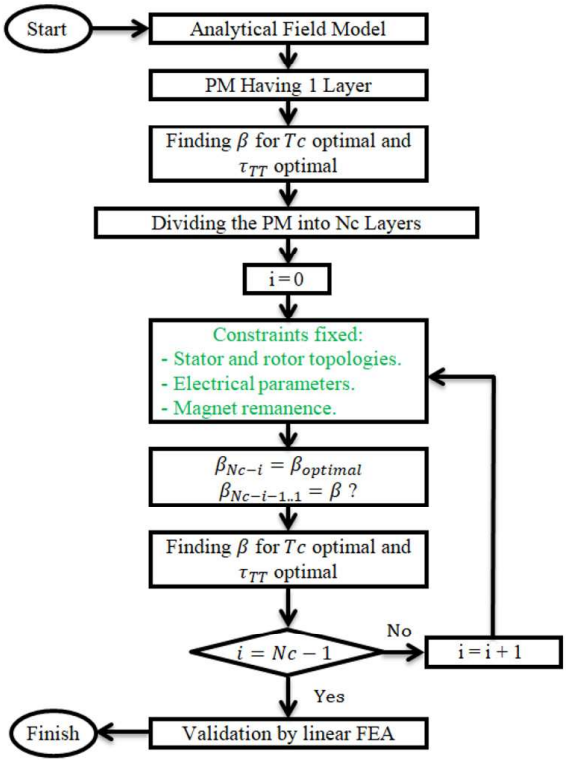

Figure 2.
Flowchart for optimal cogging torque calculation

3. Magnetic field solution

In the literature, diverse analytical, semi-analytical and numerical techniques exist to model electrical machines such as subdomain method (Boughrara *et al.*, 2012; Dubas and Boughrara, 2017), magnetic equivalent circuits, Schwarz–Christoffel conformal mapping (Boughrara *et al.*, 2009a, 2009b), hybrid analytical model (Laoubi *et al.*, 2015) and FEM. Improvements of analytical approach accuracy and precision are now firmly established goals in electrical machine design.

Figure 3 represents the schematic view of initial surface-mounted PM machine in polar coordinates. The machine is divided into four regions: magnets, air-gap, slot opening and stator slots. The dimensions and specifications of this machine are listed in Table I.

To find the analytical solution of magnetic field distribution in the different regions, it is necessary to use the method of variables separation and the boundary and interface conditions. For this, the following assumptions are made:

- Permeability of iron core is supposed to have infinite permeability.
- Conductivity of all regions is supposed negligible.
- The magnet has a radial magnetization, a linear demagnetization curve and relative permeability equal to unity.

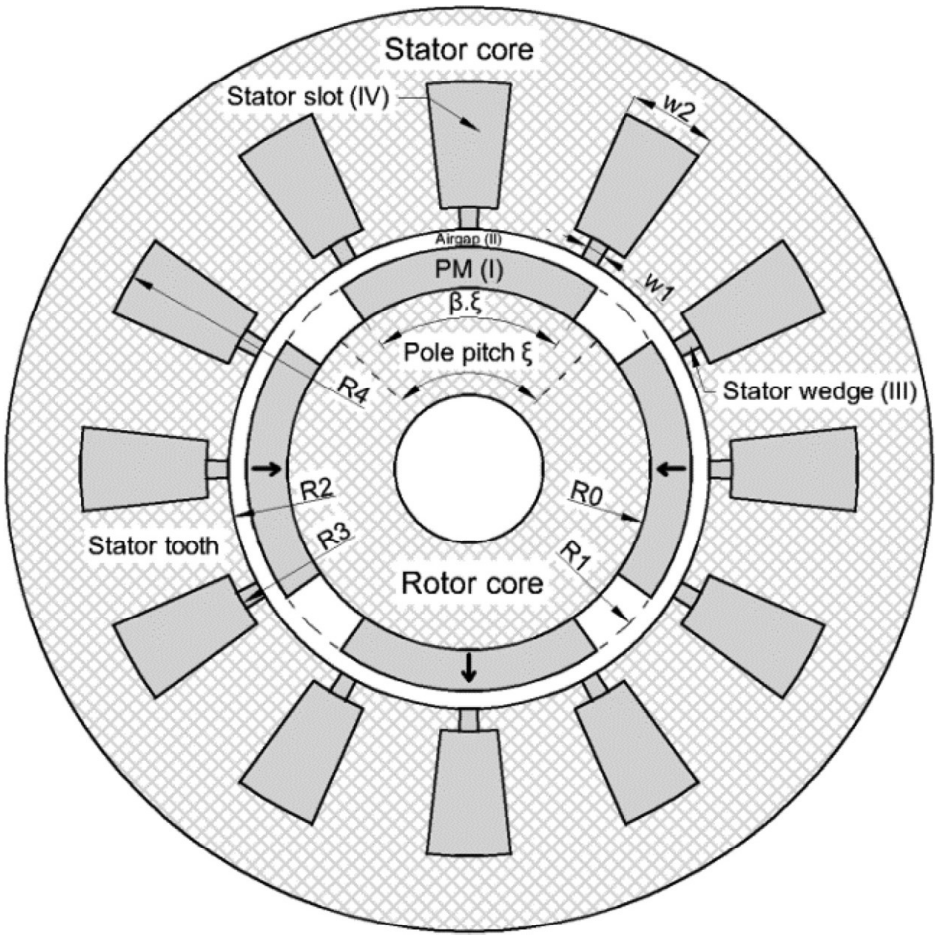

Figure 3.
Studied Surface-mounted PM machine

The magnetic field equations are solved in the polar coordinates system using magnetic vector potential $\overrightarrow{A}$ which is defined as:

$$\overrightarrow{B} = \nabla \times \overrightarrow{A} \tag{1}$$

In a continuous and isotropic region, the magnetic flux density and magnetic field vectors B and H in the regions indicated in Figure 1 are coupled by the following equations:

$$\text{Region I}: \overrightarrow{B} = \mu_0\left(\mu_r\overrightarrow{H} + \overrightarrow{M}\right) \tag{2}$$

$$\text{Regions II, III, IV}: \overrightarrow{B} = \mu_0\overrightarrow{H} \tag{3}$$

Where $\overrightarrow{M}$, μ_0, μ_r stands respectively: magnetization vector, permeability of vacuum and relative permeability. The general expression of the vector potential A distribution is written as:

$$\nabla^2\overrightarrow{A} = -\mu_0\left(\nabla \times \overrightarrow{M} + \overrightarrow{J}\right) \tag{4}$$

Where $\overrightarrow{J}$ is the exciting current density.

3.1 In Region I: R0 < r < R1

The Poisson's equation in Region I is given by:

$$\frac{\partial^2 A_j^I(r,\theta)}{\partial r^2} + \frac{1}{r}\frac{\partial A_j^I(r,\theta)}{\partial r} + \frac{1}{r^2}\frac{\partial^2 A_j^I(r,\theta)}{\partial \theta^2} = -\frac{\mu_0}{r}\left(M_{\theta j}(\theta) - \frac{\partial M_{rj}(\theta)}{\partial \theta}\right) \tag{5}$$

According to Fourier series expansion, the radial and circumferential magnetization can be written as follows:

$$M_{\theta j}(\theta) = 0 \tag{6}$$

$$M_{rj}(\theta) = \sum_{n=1,3,5}^{\infty}\left(M_{rsjn}.\cos(np.\theta) + M_{rcjn}.\sin(np.\theta)\right) \tag{7}$$

where

$$M_{rsjn} = -\frac{4B_{rm}}{n\pi\mu_0}\sin\left(\frac{n\pi}{2}\right)\sin\left(\frac{n\pi\beta(j)}{2}\right)\sin\left(\frac{n\tau}{2}\right) \tag{8}$$

$$M_{rcjn} = -\frac{4B_{rm}}{n\pi\mu_0}\sin\left(\frac{n\pi}{2}\right)\sin\left(\frac{n\pi\beta(j)}{2}\right)\cos\left(\frac{n\tau}{2}\right) \tag{9}$$

B_{rm}, $\beta(j)$, τ and p are magnet remanence, magnet arc to pole pitch ratio for the layer (j), rotor orientation angle and number of pole pairs, respectively. M_{rsjn} and M_{rcjn} are the n^{th} element of the radial component M_{rj} of magnet. The boundary condition in the first layer of magnet is given by:

$$B^{I}_{\theta 1}(r,\theta)|_{r=R0} = 0 \tag{10}$$

3.2 In Regions II, III and IV

The cogging torque and back-EMF are determined at no load, for this condition, the magnetic vector potential distribution in the airspace is governed by Laplace's equation:

$$\frac{\partial^2 A^{II,III,IV}(r,\theta)}{\partial r^2} + \frac{1}{r}\frac{\partial A^{II,III,IV}(r,\theta)}{\partial r} + \frac{1}{r^2}\frac{\partial^2 A^{II,III,IV}(r,\theta)}{\partial \theta^2} = 0 \tag{11}$$

The radial and circumferential flux densities, in each region, are described by the magnetic vector potential and are expressed as follows:

$$B_r(r,\theta) = \frac{1}{r}\frac{\partial A(r,\theta)}{\partial r} \tag{12}$$

$$B_\theta(r,\theta) = -\frac{\partial A(r,\theta)}{\partial \theta} \tag{13}$$

Laplace equation resolution is frequently achieved by using Euler–Cauchy and Sturm–Liouville methods, while the resolution of Poisson equation is achieved by using Green method (Jeffrey, 2002).

Considering the periodicity condition at $2\pi/p$, the general solution of magnetic vector potential in the Region I can be written as follows in equation (14):

$$A^{I}_{j}(r,\theta) = \sum_{n=1}^{nh}\left(C^{I}_{j3n}r^{np} + C^{I}_{j4n}r^{-np} + \Gamma s_j(r)\right) \times \sin(np.\theta) + \sum_{n=1}^{nh}\left(C^{I}_{j5n}r^{np} + C^{I}_{j6n}r^{-np} + \Gamma c_j(r)\right) \times \cos(np.\theta) \tag{14}$$

where:

$$\Gamma s_j(r) = \begin{cases} +\dfrac{np \cdot Mrsjn}{(np)^2 - 1}r & if\ np \neq 1 \\ +\dfrac{Mrsj1}{2}r \cdot \ln(r) & if\ np = 1 \end{cases} \tag{15}$$

$$\Gamma c_j(r) = \begin{cases} -\dfrac{np \cdot Mrcjn}{(np)^2 - 1}r & if\ np \neq 1 \\ -\dfrac{Mrcj1}{2}r \cdot \ln(r) & if\ np = 1 \end{cases} \tag{16}$$

$\Gamma_{s\,j}(r)$ and $\Gamma c_j(r)$ are the particular solution of equation (5).

The solution of magnetic vector potential in Region II is given in equation (17), where its periodicity condition is equal to $2\pi/p$:

$$A^{II}(r,\theta) = \sum_{n=1}^{nh}\left(C_{3n}^{II} r^{np} + C_{4n}^{II} r^{-np}\right) \times \sin(np.\theta) + \sum_{n=1}^{nh}\left(C_{5n}^{II} r^{np} + C_{6n}^{II} r^{-np}\right) \times \cos(np.\theta) \tag{17}$$

In Region III, considering boundary condition from equation (18), magnetic vector magnetic potential can be expressed as follows in equation (19):

$$B_{ri}^{III}(r,\theta) = 0\big|^{\theta = g_i \pm {}^{w1}/_{2}} \tag{18}$$

$$A_i^{III}(r,\theta) = C_{i1}^{III}\ln(r) + C_{i2}^{III} + \sum_{m=1}^{nh}\left(C_{i3m}^{III} r^{\frac{m\pi}{w1}} + C_{i4m}^{III} r^{-\frac{m\pi}{w1}}\right) \times \cos\left(\frac{m\pi}{w1}\left(\theta - g_i + {}^{w1}/_{2}\right)\right) \tag{19}$$

$w1, g_i$ are respectively slot opening, the angular position of the ith slot in radians.

The same method for the Region III is used to find the solution in Region IV by taking into account the boundary conditions of equations (20) and (21):

$$B_{ri}^{IV}(r,\theta) = 0\big|^{\theta = g_i \pm {}^{w2}/_{2}} \tag{20}$$

$$B_{\theta i}^{IV}(r,\theta) = 0\big|_{r=R4} \tag{21}$$

$$A_i^{IV}(r,\theta) = C_{i2}^{IV} + \sum_{k=1}^{nh} C_{i4k}^{IV}\left(R4^{-\frac{2k\pi}{w2}} r^{\frac{k\pi}{w2}} + r^{-\frac{k\pi}{w2}}\right) \times \cos\left(\frac{k\pi}{w2}\left(\theta - g_i + {}^{w2}/_{2}\right)\right) \tag{22}$$

$w2$ is stator slot opening, supposed equal to two-third of slot pitch.

The constants $C^{I,II,III,IV}$ should be determined by applying interface conditions. These interfaces must satisfy the continuity of the radial component of the flux density and the continuity of the circumferential component of the magnetic field (the detailed calculation method is given in the Appendix):

$$\left(H_{\theta i}^{IV}(r,\theta) = H_{\theta i}^{III}(r,\theta)\right)\Big|_{r=R3}^{g_i - {}^{w1}/_{2} \le \theta \le g_i + {}^{w1}/_{2}} \tag{23}$$

$$\left(B_{ri}^{IV}(r,\theta) = B_{ri}^{III}(r,\theta)\right)\Big|_{r=R3}^{g_i - {}^{w1}/_{2} \le \theta \le g_i + {}^{w1}/_{2}} \tag{24}$$

$$\left(B_r^{II}(r,\theta) = B_{ri}^{III}(r,\theta)\right)\Big|_{r=R2}^{g_i - {}^{w1}/_2 \le \theta \le g_i + {}^{w1}/_2} \tag{25}$$

$$\left(H_\theta^{II}(r,\theta) = \sum_{i=1}^{Qs} H_{\theta i}^{III}(r,\theta)\right)\Big|_{r=R2} \tag{26}$$

Where Qs represents the number of stator slots and subscript i denotes the ith slot:

$$\left(B_r^{II}(r,\theta) = B_{rNc}^{I}(r,\theta)\right)\Big|_{r=R1} \tag{27}$$

$$\left(H_\theta^{II}(r,\theta) = H_{\theta Nc}^{I}(r,\theta)\right)\Big|_{r=R1} \tag{28}$$

$$\left(B_{rj}^{I}(r,\theta) = B_{r(j+1)}^{I}(r,\theta)\right)\Big|_{r=Ra(j)} \tag{29}$$

$$\left(H_{\theta j}^{I}(r,\theta) = H_{\theta(j+1)}^{I}(r,\theta)\right)\Big|_{r=Ra(j)} \tag{30}$$

Where $Ra(j)$ represents magnet radius in the layer j.

Figures 4 and 5 show the distribution of radial and circumferential flux density issued by analytical model in the center of the air-gap for a machine having $2p = 6$, $Qs = 36$ with the same dimensions indicated in Table I.

4. Torque and back-EMF calculation

4.1 Cogging torque

On the open circuit, the cogging torque is derived by using the Maxwell's stress tensor theory:

$$T_c = \frac{L_u R^2}{\mu_0}\int_0^{2\pi} B_r^{II}(r,\theta) \times B_\theta^{II}(r,\theta).d\theta \tag{31}$$

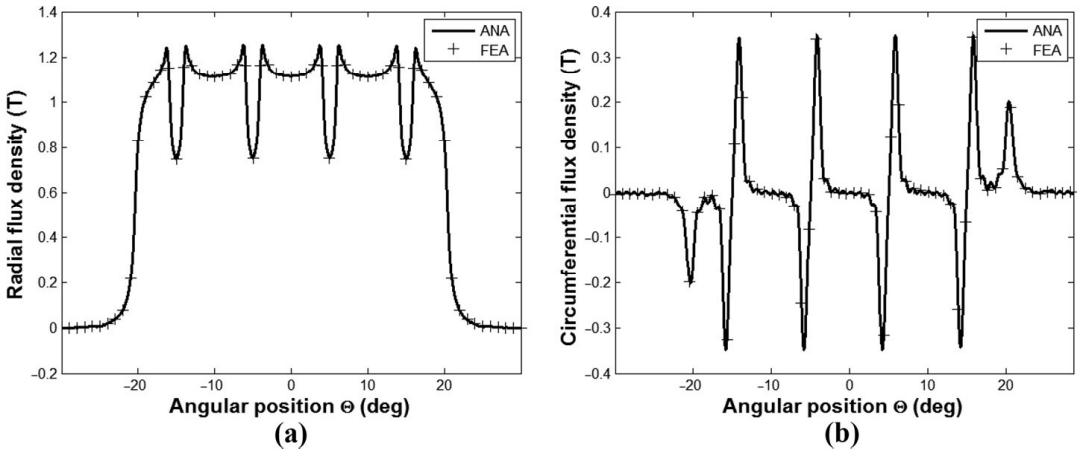

Figure 4.
(a) Radial and (b) circumferential components of the flux density in the middle of air-gap for $2p = 6$, $Qs = 36$ (1 layer: $\beta_1 = 68$ per cent)

Where L_u, R are, respectively, the axial length of the motor and the radius of a circle situated at the middle of the air-gap. The number of steps for calculating the cogging torque is equal to 20 for any machine dimensions and parameters.

4.2 Back EMF

The back-EMF calculation, is based on the Stokes theorem, it is given by the rate of change of flux linkage according to time variation. The flux per slot is given by:

$$\phi_i^{IV} = \frac{N_s L_u}{S} \int_{g_{i-w2}/2}^{g_{i+w2}/2} \int_{R_3}^{R_4} A_i^{IV}(r, \theta) \cdot r \cdot dr \cdot d\theta \tag{32}$$

Where S, Ns are the cross-section area of the stator slots and the number of series turns per slot respectively. The flux linkage per phase, created by PMs, is given by:

$$\psi_{A,B,C}^{IV} = Cm\,\phi_i^{IV} \tag{33}$$

Where Cm is the connecting matrix that represents the distribution of stator single-layer windings placed inside the slots. The three phase's back-EMF can be calculated by:

$$E_{A,B,C} = \Omega r \frac{d\psi_{A,B,C}^{IV}}{d\tau} \tag{34}$$

Where Ωr is the rotor angular speed.

4.3 Electromagnetic torque

The electromagnetic torque T_{em} can be expressed as follow:

$$T_{em} = \frac{E_A I_A + E_B I_B + E_C I_C}{\Omega_r} \tag{35}$$

The instantaneous torque output (TT) of a three-phase PMSM, can be derived by ignoring the saturation of the magnetic circuit and leakage inductance, is defined as the sum of electromagnetic torque (T_{em}) and cogging torque (T_c):

$$TT = T_{em} + T_c \tag{36}$$

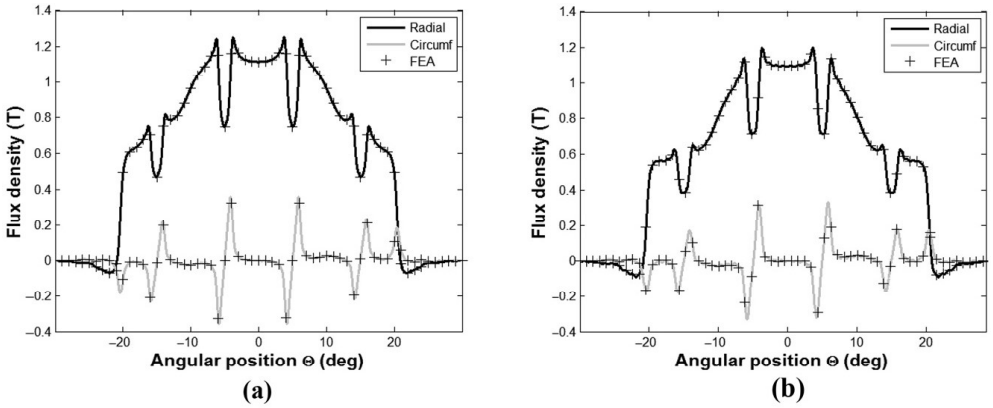

Figure 5.
Radial and circumferential components of the flux density in the middle of air-gap for $2p = 6$, $Qs = 36$

Notes: (a) 3 layers: $\beta_{1,2,3}$ = 59,35,68 per cent; (b) 6 layers: $\beta_{1,2,3,4,5,6}$ = 21,61,35,35,68,68 per cent

For the machine having $2p = 6$, $Qs = 36$ and the same parameters are indicated in Table I. The optimal opening of the magnet for original design is equal to 68 per cent of the pole pitch. The value of the cogging torque is equal to 0.95 Nm. To reduce the magnitude of cogging torque in this example, the magnet is divided into three layers. First, the magnet arc to pole pitch ratio for all magnet layers is equal to $\beta = 68$ per cent. The second stage is to find the optimal opening β_2 of the second and first layer at the same time, and if the value of $\beta_{Nc} = 68$ per cent, it is equal to 35 per cent. The magnitude of the cogging torque is equal to 0.14 Nm. Consequently, a reduction of 85 per cent compared to the previous case is reached. The arc to pole pitch ratio value of the first layer is equal to 59 per cent; this value is determined by respecting $\beta_{Nc} = 68$ per cent and $\beta_2 = 35$ per cent as shown in Figure 6. It is found that the magnitude of cogging torque decreases from 0.14 Nm toward 0.07 Nm. Consequently, another reduction of 50 per cent compared to the previous case. Figure 6 shows that the cogging torque per unit is compared toward rated torque where its value is equal to 10 Nm.

The sinusoidal stator current magnitude of the proposed machine is selected equal to 1A so that the effect of the cogging torque on the torque (TT) will be remarkable. It can be seen that the torque ripple is also affected by the reduction to 107 per cent toward 16 per cent, consequently, reduction of 85 per cent is remarked.

To protect the final layer, for this example, against rupture; it is necessary to make a non-magnetic base (Figure 7).

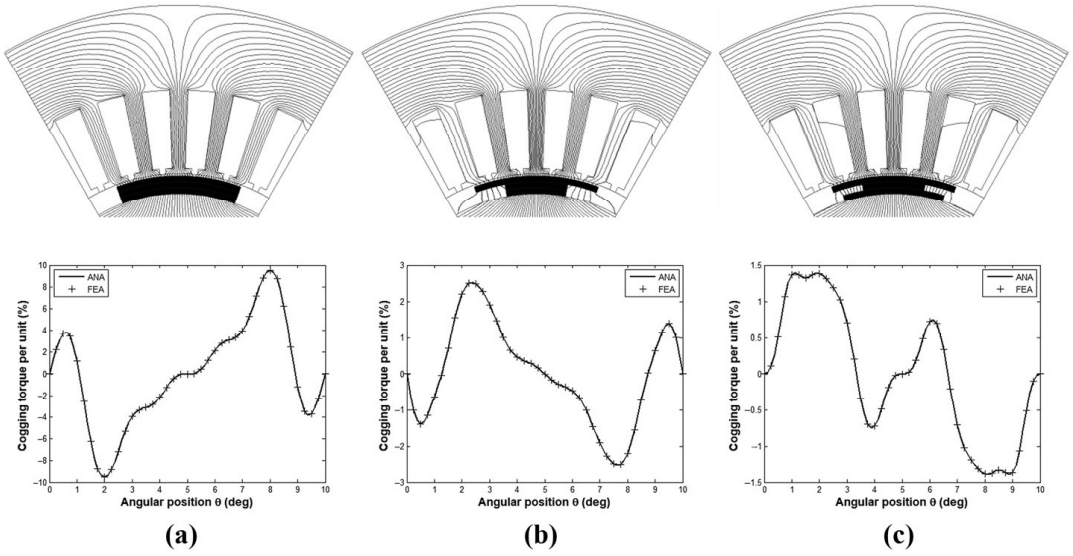

Notes: (a) Step1: $\beta_{1,2,3} = 68,68,68$ per cent; (b) Step2: $\beta_{1,2,3} = 35,35,68$ per cent; (c) Step3: $\beta_{1,2,3} = 59,35,68$ per cent

Figure 6. Influence of magnet step on cogging torque for $2p = 6$, $Qs = 36$

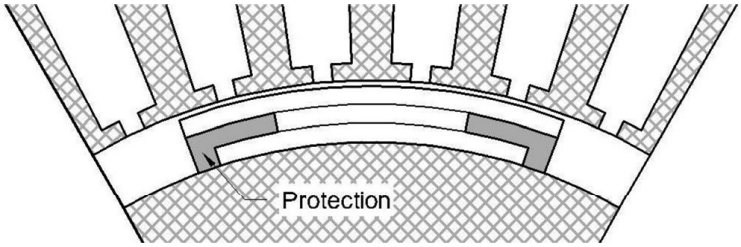

Figure 7. Protection of the final magnet layer against rupture

Table II.
Analytical results of torque

	$2p = 4$, $Qs = 36$				$2p = 6$, $Qs = 36$			
	1 layer	3 layers	6 layers	SPM	1 layer	3 layers	6 layers	SPM
Magnet arc to pole pitch ratio β_{1Nc} (%)	90	63, 45, 90	63, 45, 45, 45, 56, 90	55	68	59, 35, 68	61, 32, 35, 35, 68, 68	81
Volume of magnet (m^3) $\times 10^{-6}$	83.7	61.7	53.6	33.7	42.2	33.6	31	33
Cogging torque (T_c) optimal (Nm)	1.09	0.18	*0.04*	*0.13*	*0.95*	*0.14*	*0.07*	*0.22*
Electromagnetic torque (T_{em}) ripple (%)	9.67	6.81	5.52	6.55	14.54	9.34	7.38	1.93
Total torque (TT) mean (Nm)	2.28	1.91	1.75	0.80	2.04	1.71	1.59	1.63
Total torque (TT) ripple (%)	*102.77*	*21.08*	*8.15*	*38.72*	*107.38*	*24.93*	*15.74*	*28.99*
Total torque (TT) ripple/volume of magnets (Nm/m^3)	6,810	7,739	8,162	5,935	8,057	8,482	8,548	8,232
	$2p = 8$, $Qs = 72$				$2p = 4$, $Qs = 24$			
	1 layer	3 layers	6 layers	SPM	1 layer	3 layers	6 layers	SPM
Magnet arc to pole pitch ratio β_{1Nc} (%)	57	54, 43, 57	51, 51, 49, 36, 46, 57	100	84	86, 85, 84	87, 86, 85, 85, 84, 84	78
Volume of magnet (m^3) x10^{-6}	26.5	23.9	22.5	30.0.8	78.1	79.1	79.2	47.3
Cogging torque (T_c) optimal (Nm)	*1.2*	*0.26*	*0.13*	*0.30*	*0.90*	*0.26*	*0.21*	*0.07*
Electromagnetic torque (T_{em}) ripple (%)	8.66	6.00	3.87	0.27	7.91	7.94	7.97	3.33
Total torque (TT) mean (Nm)	3.56	3.28	3.12	4.85	1.51	1.51	1.51	0.71
Total torque (TT) ripple (%)	*76.43*	*21.60*	*12.22*	*12.42*	*121*	*36.50*	*29.53*	*23.30*
Total torque (TT) ripple/volume of magnets ($N.m/m^3$)	16,792	17,154	17,333	19,683	4,833	4,772	4,766	3,753

Table II shows the values of the optimal magnitude of cogging torque and torque ripple for different machine related to the 1, 3 and 6 layers. The single layer distributed winding is chosen where the number of the turns per slot is equal to 10.

From the analysis of Table II, we can confirm that this new technique can improve considerably the machine performances in terms to reduce the cogging torque peak or torque ripple. The ratio total torque/volume of magnets is proportional to the number of magnet layers. In all circumstances, the magnet having six layers exhibits good results in contrast to the machine having three layers. We can remark also that some machines exhibit good results compared to sinusoidal magnet shape SPM (for example $2p = 4$, $Qs = 36$ or $2p = 6$, $Qs = 36$) whether for three or six layers.

The linear finite element analysis (FEA) model is used (Meeker, 2010) and compared with the foregoing developed analytical approach. Figure 8 shows equal distribution of flux density for a machine having $2p = 4$, $Qs = 36$ and $2p = 6$, $Qs = 36$; the number of magnet layers is equal to 6. The magnet arc to pole pitch ratio of each magnet layer is indicated in Table II (Figure 9).

5. Conclusion

A new technique based on analytical method is presented to improve machine surface-mounted permanent magnet synchronous machine performances taking into account of magnet shaping. It shows that the proposed classical permanent magnet shape divided into small number of layers can effectively reduce greatly the cogging torque peak and torque ripple whatever the number of pole pairs or slots. Accurate results are obtained for different machines and compared against linear FEA. The proposed model is also compared with sinusoidal PM and gives excellent results.

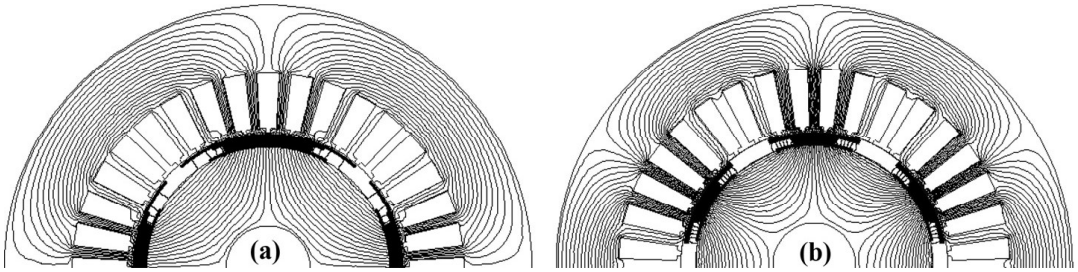

Figure 8.
Equal distribution of flux density for a machine having: (a) $2p = 4$, $Qs = 36$, (b) $2p = 6$, $Qs = 36$ with optimal magnet opening (six layers)

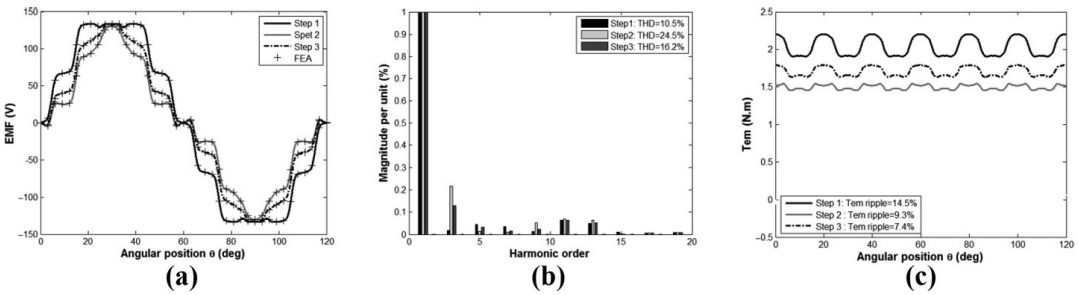

Figure 9.
(a) Back-EMF, (b) Harmonics for Back-EMF and (c) electromagnetic torque for $2p = 6$, $Qs = 36$ (three layers) after 1st, 2nd and 3rd configuration stages

References

Ashabani, M., Abdel-Rady, Y. and Mohamed, I. (2011), "Multi-objective shape optimization of segmented pole permanent-magnet synchronous machines with improved torque characteristics", *IEEE Transactions on Magnetics*, Vol. 47 No. 4, pp. 795-804.

Boughrara, K., Ibtiouen, R. and Lubin, T. (2012), "Analytical prediction of magnetic field in parallel double excitation and spoke-type permanent-magnet machines accounting for tooth-tips and shape of polar pieces", *IEEE Transactions on Magnetics*, Vol. 48 No. 7, pp. 2121-2137.

Boughrara, K.L., Chikouche, B., Ibtiouen, R., Zarko, D. and Touhami, O. (2009a), "Analytical analysis of slotted air-gap surface mounted permanent-magnet synchronous motor with magnet bars magnetized in shifting direction", *IEEE Transactions on Magnetics*, Vol. 45 No. 2, pp. 747-758.

Boughrara, K., Zarko, D., Ibtiouen, R., Touhami, O. and Rezzoug, A. (2009b), "Magnetic field analysis of inset and surface-mounted permanent-magnet synchronous motors using Schwarz–Christoffel transformation", *IEEE Transactions on Magnetics*, Vol. 45 No. 8, pp. 3166-3178.

Dubas, F. and Boughrara, K. (2017), "New scientific contribution on the 2-D subdomain technique in Cartesian coordinates: taking into account of iron parts", *Mathematical and Computational Applications MDPI*, Vol. 22 No. 1, p. 17, doi: 10.3390/mca22010017.

Fei, W. and Luk, P.C.K. (2012), "Torque ripple reduction of a direct-drive permanent-magnet synchronous machine by material-efficient axial pole pairing", *IEEE Transactions on Industrial Electronics*, Vol. 59 No. 6, pp. 2601-2611.

Gong, J., Aslan, B., Gillon, F. and Semail, E. (2014), "High-speed functionality optimization of five-phase PM machine using third harmonic current", *Compel – The International Journal for Computation and Mathematics in Electrical and Electronic Engineering*, Vol. 33 No. 3, pp. 879-893.

Gu, Z.Y., Wang, K., Zhu, Z.Q., Wu, Z.Z., Liu, C. and Cao, R.W. (2018), "Torque improvement in five-phase unequal tooth spm machine by injecting third harmonic current", *IEEE Transactions on Vehicular Technology*, Vol. 67 No. 1, pp. 206-215.

Houari, A., Bouabdallah, A., Djerioui, A., Machmoum, M. and Auger, (2018), "An effective compensation technique for speed smoothness at low-speed operation of PMSM drives", *IEEE Transactions on Industry Applications*, Vol. 54 No. 1, pp. 647-655.

Islam, M., S., Mir, S. and Sebastian, T. (2004), "Issues in reducing the cogging torque of mass-produced permanent-magnet brushless DC motor", *IEEE Transactions on Industry Applications*, Vol. 40 No. 3, pp. 813-820.

Jang, S.-M., Park, H.-I., Choi, J.-Y., Ko, K.-J. and Lee, S.-H. (2011), "Magnet pole shape design of permanent magnet machine for minimization of torque ripple based on electromagnetic field theory", *IEEE Transactions on Magnetics*, Vol. 47 No. 10, pp. 3586-3589.

Jeffrey, A. (2002), *Advanced Engineering Mathematics*, University of Newcastle-upon-Tyne, Harcourt/ Academic Press, Newcastle upon Tyne.

Laoubi, Y., Dhifli, M., Verez, G., Amara, Y. and Barakat, G. (2015), "Open circuit performance analysis of a permanent magnet linear machine using a new hybrid analytical model", *IEEE Transactions on Magnetics*, Vol. 51 No. 3, pp. 1-3, doi: 10.1109/TMAG.2014.2361017.

Laskaris, K.I. and Kladas, A.G. (2011), "Permanent-magnet shape optimization effects on synchronous motor performance", *IEEE Transactions on Industrial Electronics*, Vol. 58 No. 9, pp. 3776-3783.

Lateb, R., Takorabet, N. and Meibody-Tabar, F. (2006), "Effect of magnet segmentation on the cogging torque in surface-mounted permanent-magnet motors", *IEEE Transactions on Magnetics*, Vol. 42 No. 3, pp. 442-445.

Meeker, D.C. (2010), "Finite element method magnetics, version 4.2, Build", available at: www.femm.info.

Oner, Y., Zhu, Z.Q., Wu, L.J. and Ge, X. (2015), "Analytical Sub-domain model for predicting open-circuit field of permanent magnet vernier machine accounting for tooth tips", *Compel – The International Journal for Computation and Mathematics in Electrical and Electronic Engineering*, Vol. 35 No. 2, pp. 624-640.

Sadeghi, S. and Parsa, L. (2012), "Improved technique for minimizing torque pulsation in Halbach array permanent magnet machines", *Compel – The International Journal for Computation and Mathematics in Electrical and Electronic Engineering*, Vol. 31 No. 6, pp. 1590-1602.

Sung, S.J., Park, S.J. and Jang, G.H. (2011), "Cogging torque of brushless DC motors due to the interaction between the uneven magnetization of a permanent magnet and teeth curvature", *IEEE Transactions on Magnetics*, Vol. 47 No. 7, pp. 1923-1928.

Wang, D., Wang, X. and Jung, S.Y. (2013), "Cogging torque minimization and torque ripple suppression in surface-mounted permanent magnet synchronous machines using different magnet widths", *IEEE Transactions on Magnetics*, Vol. 49 No. 5, pp. 2295-2298.

Wang, K., Zhu, Z.Q. and Ombach, G. (2014a), "Torque enhancement of surface-mounted permanent magnet machine using third-order harmonic", *IEEE Transactions on Magnetics*, Vol. 50 No. 3, pp. 104-113, doi: 10.1109/TMAG.2013.2286780.

Wang, K., Zhu, Z.Q., Ombach, G., Koch, M., Zhang, S. and Xu, J. (2014b), "Electromagnetic performance of an 18-slot/10-pole fractional-slot surface-mounted permanent-magnet machine", *IEEE Transactions on Industry Applications*, Vol. 50 No. 6, pp. 3685-3696.

Xia, C., Zhang, Z. and Geng, Q. (2015), "Analytical modeling and analysis of surface mounted permanent magnet machines with skewed slots", *IEEE Transactions on Magnetics*, Vol. 51 No. 5, pp. 1-8, doi: 10.1109/TMAG.2014.2364156.

Xintong, J., Jingwei, X., Yong, L. and Yongping, L. (2009), "Theoretical and simulation analysis of influences of stator tooth widthon cogging torque of BLDC motors", *IEEE Transactions on Magnetics*, Vol. 45 No. 10, pp. 4601-4604.

Zhao, P. and Yang, G. (2011), "Torque density improvement of five-phase PMSM drive for electric vehicles applications", *Journal of Power Electronics*, Vol. 11 No. 4, pp. 401-407.

Zhu, Z.Q. (2015), "Fractional slot permanent magnet brushless machines and drives for electric and hybrid propulsion systems", *Compel – The International Journal for Computation and Mathematics in Electrical and Electronic Engineering*, Vol. 30 No. 1, pp. 9-31.

Appendix

Radial and circumferential flux densities components, in each region, are expressed as:

Region I:

$$B_{rj}^{I}(r,\theta)=\frac{1}{r}\sum_{n=1}^{nh}np\left(C_{j3n}^{I}r^{np}+C_{j4n}^{I}r^{-np}+\Gamma s_j(r)\right)\times\cos(np.\theta)-\frac{1}{r}\sum_{n=1}^{nh}np\left(C_{j5n}^{I}r^{np}+C_{j6n}^{I}r^{-np}+\Gamma c_j(r)\right)\times\sin(np.\theta) \tag{A1}$$

$$H_{\theta j}^{I}(r,\theta)=-\sum_{n=1}^{nh}\left(np\left(C_{j3n}^{I}r^{np-1}-C_{j4n}^{I}r^{-np-1}\right)+\frac{d}{dr}\left(\Gamma s_j(r)\right)\right)\times\sin(np.\theta)-\sum_{n=1}^{nh}\left(np\left(C_{j5n}^{I}r^{np-1}-C_{j6n}^{I}r^{-np-1}\right)+\frac{d}{dr}\left(\Gamma c_j(r)\right)\right)\times\cos(np.\theta) \tag{A2}$$

Region II:

$$B_{r}^{II}(r,\theta)=\frac{1}{r}\sum_{n=1}^{nh}np\left(C_{3n}^{II}r^{np}+C_{4n}^{II}r^{-np}\right)\times\cos(np.\theta)-\frac{1}{r}\sum_{n=1}^{nh}np\left(C_{5n}^{II}r^{np}+C_{6n}^{II}r^{-np}\right)\times\sin(np.\theta) \tag{A3}$$

$$H_{\theta i}^{II}(r,\theta) = -\sum_{n=1}^{nh} np\left(C_{3n}^{II} r^{np-1} - C_{4n}^{II} r^{-np-1}\right) \times \sin(np.\theta) - \sum_{n=1}^{nh} np\left(C_{5n}^{II} r^{np-1} - C_{6n}^{II} r^{-np-1}\right) \times \cos(np.\theta) \quad \text{(A4)}$$

Region III:

$$B_{ri}^{III}(r,\theta) = -\frac{1}{r}\sum_{m=1}^{nh} \frac{m\pi}{w1}\left(C_{i3m}^{III} r^{\frac{m\pi}{w1}} + C_{i4m}^{III} r^{-\frac{m\pi}{w1}}\right) \times \sin\left(\frac{m\pi}{w1}\left(\theta - g_i + {}^{w1}/_{2}\right)\right) \quad \text{(A5)}$$

$$H_{\theta i}^{III}(r,\theta) = -\frac{1}{r}C_{i1}^{III} - \sum_{m=1}^{nh} \frac{m\pi}{w1}\left(C_{i3m}^{III} r^{\frac{m\pi}{w1}-1} - C_{i4m}^{III} r^{-\frac{m\pi}{w1}-1}\right) \times \cos\left(\frac{m\pi}{w1}\left(\theta - g_i + {}^{w1}/_{2}\right)\right) \quad \text{(A6)}$$

Region IV:

$$B_{ri}^{IV}(r,\theta) = -\frac{1}{r}\sum_{k=1}^{nh} \frac{k\pi}{w2} C_{i4k}^{IV}\left(R4^{-\frac{2k\pi}{w2}} r^{\frac{k\pi}{w2}} + r^{-\frac{k\pi}{w2}}\right) \times \sin\left(\frac{k\pi}{w2}\left(\theta - g_i + {}^{w2}/_{2}\right)\right) \quad \text{(A7)}$$

$$H_{\theta i}^{IV}(r,\theta) = -\sum_{m=1}^{nh} \frac{k\pi}{w2} C_{i4k}^{IV}\left(R4^{-\frac{2k\pi}{w2}} R3^{\frac{k\pi}{w2}-1} - R3^{-\frac{k\pi}{w2}-1}\right) \times \cos\left(\frac{k\pi}{w2}\left(\theta - g_i + {}^{w2}/_{2}\right)\right) \quad \text{(A8)}$$

The Fourier coefficients $C^{I,II,III,IV}$ can be calculated as:

From Equation (10), we get:

$$np\left(C_{13n}^{I} R0^{np-1} - C_{14n}^{I} R0^{-np-1}\right) + \frac{d}{dr}\left(\Gamma s_1(R0)\right) = 0 \quad \text{(A9)}$$

$$np\left(C_{15n}^{I} R0^{np-1} - C_{16n}^{I} R0^{-np-1}\right) + \frac{d}{dr}\left(\Gamma c_1(R0)\right) = 0 \quad \text{(A10)}$$

From Equation (23), we have:

$$-\frac{1}{R3}C_{i1}^{III} = \frac{1}{w1}\int_{g_i - {}^{w1}/_{2}}^{g_i + {}^{w1}/_{2}} H_{\theta i}^{IV}(R3,\theta)d\theta \quad \text{(A11)}$$

$$-\frac{m\pi}{w1}\left(C_{i3m}^{III}R3^{\frac{m\pi}{w1}-1}-C_{i4m}^{III}R3^{-\frac{m\pi}{w1}-1}\right)=\frac{2}{w1}\int_{g_i-{}^{w1}/_2}^{g_i+{}^{w1}/_2}H_{\theta i}^{IV}(R3,\theta)\times\cos\left(\frac{m\pi}{w1}\left(\theta-g_i+{}^{w1}/_2\right)\right)d\theta \tag{A12}$$

From (24), we get:

$$-\frac{1}{R3}\frac{k\pi}{w2}C_{i4k}^{IV}\left(R4^{-\frac{2k\pi}{w2}}R3^{\frac{k\pi}{w2}}+R3^{-\frac{k\pi}{w2}}\right)=\frac{2}{w1}\int_{g_i-{}^{w1}/_2}^{g_i+{}^{w1}/_2}B_{ri}^{III}(R3,\theta)\times\sin\left(\frac{k\pi}{w2}\left(\theta-g_i+{}^{w2}/_2\right)\right)d\theta \tag{A13}$$

Development of (25) gives:

$$-\frac{1}{R2}\frac{m\pi}{w1}\left(C_{i3m}^{III}R2^{\frac{m\pi}{w1}}+C_{i4m}^{III}R2^{-\frac{m\pi}{w1}}\right)=\frac{2}{w1}\int_{g_i-{}^{w1}/_2}^{g_i+{}^{w1}/_2}B_{ri}^{II}(R2,\theta)\times\sin\left(\frac{m\pi}{w1}\left(\theta-g_i+{}^{w1}/_2\right)\right)d\theta \tag{A14}$$

From Equation (26), we get:

$$-np\left(C_{3n}^{II}R2^{np-1}-C_{4n}^{II}R2^{-np-1}\right)=\frac{2p}{\pi}\sum_{i=1}^{Qs}\int_{g_i-{}^{w1}/_2}^{g_i+{}^{w1}/_2}H_{\theta i}^{II}(R2,\theta)\times\sin(np.\theta)d\theta \tag{A15}$$

$$-np\left(C_{5n}^{II}R2^{np-1}-C_{6n}^{II}R2^{-np-1}\right)=\frac{2p}{\pi}\sum_{i=1}^{Qs}\int_{g_i-{}^{w1}/_2}^{g_i+{}^{w1}/_2}H_{\theta i}^{II}(R2,\theta)\times\cos(np.\theta)d\theta \tag{A16}$$

From (27), we have:

$$C_{3n}^{II}R1^{np}+C_{4n}^{II}R1^{-np}=C_{Nc3n}^{I}R1^{np}+C_{Nc4n}^{I}R1^{-np}+\Gamma s_{Nc}(R1) \tag{A17}$$

$$C_{5n}^{II}R1^{np}+C_{6n}^{II}R1^{-np}=C_{Nc5n}^{I}R1^{np}+C_{Nc6n}^{I}R1^{-np}+\Gamma c_{Nc}(R1) \tag{A18}$$

Development of (28) gives:

$$np\left(C_{3n}^{II}R1^{np-1}-C_{4n}^{II}R1^{-np-1}\right)=np\left(C_{Nc3n}^{I}R1^{np-1}-C_{Nc4n}^{I}R1^{-np-1}\right)+\frac{d}{dr}\left(\Gamma s_{Nc}(R1)\right) \tag{A19}$$

$$np\left(C_{5n}^{II}R1^{np-1}-C_{6n}^{II}R1^{-np-1}\right)=np\left(C_{Nc5n}^{I}R1^{np-1}-C_{Nc6n}^{I}R1^{-np-1}\right)+\frac{d}{dr}\left(\Gamma c_{Nc}(R1)\right) \tag{A20}$$

From Equation (29), we get:

$$C_{j3n}^{I}Ra(j)^{np}+C_{j4n}^{I}Ra(j)^{-np}+\Gamma s_j(Ra(j))=C_{(j+1)3n}^{I}Ra(j)^{np}+C_{(j+1)4n}^{I}Ra(j)^{-np}+\Gamma s_{(j+1)}(Ra(j)) \tag{A21}$$

$$C_{j5n}^{I}Ra(j)^{np}+C_{j6n}^{I}Ra(j)^{-np}+\Gamma c_j(Ra(j))=C_{(j+1)5n}^{I}Ra(j)^{np}+C_{(j+1)6n}^{I}Ra(j)^{-np}+\Gamma c_{(j+1)}(Ra(j)) \tag{A22}$$

From (30), we have:

$$\begin{aligned}&np\left(C_{j3n}^{I}Ra(j)^{np-1}-C_{j4n}^{I}Ra(j)^{-np-1}\right)+\frac{d}{dr}\left(\Gamma s_j(Ra(j))\right)\\&=np\left(C_{(j+1)3n}^{I}Ra(j)^{np-1}-C_{(j+1)4n}^{I}Ra(j)^{-np-1}\right)+\frac{d}{dr}\left(\Gamma s_{(j+1)}(Ra(j))\right)\end{aligned} \tag{A23}$$

$$\begin{aligned}&np\left(C_{j5n}^{I}Ra(j)^{np-1}-C_{j6n}^{I}Ra(j)^{-np-1}\right)+\frac{d}{dr}\left(\Gamma c_j(Ra(j))\right)\\&=np\left(C_{(j+1)5n}^{I}Ra(j)^{np-1}-C_{(j+1)6n}^{I}Ra(j)^{-np-1}\right)+\frac{d}{dr}\left(\Gamma c_{(j+1)}(Ra(j))\right)\end{aligned} \tag{A24}$$

The linear system of equations to solve is constituted to 16 equations from (A9) to (A24).

Corresponding author
Brahim Ladghem Chikouche can be contacted at: lchbrahim@gmail.com